JPhys Photonics

1.3-μm passively mode-locked quantum dot lasers epitaxially grown on silicon: gain properties and optical feedback stabilization

IOP Publishing J. Phys. Photonics 2 (2020) 045006 https://doi.org/10.1088/2515-7647/aba5a6

Journal of Physics: Photonics

1.3-μm passively mode-locked quantum dot lasers epitaxially grown on silicon: gain properties and optical feedback stabilization

Bozhang Dong[1], **Xavier C de Labriolle**[1], **Songtao Liu**[2,4], **Mario Dumont**[2,4], **Heming Huang**[1], **Jianan Duan**[1], **Justin C Norman**[2,3], **John E Bowers**[2,3,4] **and Frédéric Grillot**[1,5]

[1] LTCI, Télécom Paris, Institut Polytechnique de Paris, 19 Place Marguerite Perey, 91120 Palaiseau, France
[2] Institute for Energy Efficiency , University of California, Santa Barbara, California 93106, United States of America
[3] Materials Department, University of California, Santa Barbara, California 93106, United States of America
[4] Department of Electrical and Computer Engineering, University of California, Santa Barbara, California 93106, United States of America
[5] Center for High Technology Materials, University of New-Mexico, Albuquerque, New-Mexico, 87106, United States of America

E-mail: bozhang.dong@telecom-paris.fr

OPEN ACCESS

RECEIVED
24 April 2020

REVISED
30 June 2020

ACCEPTED FOR PUBLICATION
14 July 2020

PUBLISHED
21 August 2020

Keywords: quantum dot, silicon photonics, mode-locked laser, linewidth enhancement factor, optical feedback, RF linewidth, photonics integrated circuits

Abstract

This work reports on an investigation of the optical feedback in an InAs/InGaAs passively mode-locked quantum dot (QD) laser epitaxially grown on silicon. Under the stably-resonant optical feedback condition, experiments demonstrate that the radio-frequency linewidth is narrowed whatever the bias voltage applied on the saturable absorber (SA) is; on the other hand, the effective linewidth enhancement factor of the device increases with the reverse bias voltage on the SA, hence it is observed that such an increase influences the mode-locking dynamic and the stability of device under optical feedback. This work gives insights for stabilizing epitaxial QD mode-locked lasers on silicon which is meaningful for their applications in future large-scale silicon electronic and photonic applications requiring low power consumption as well as for high-speed photonic analog-to-digital conversion, intrachip/interchip optical clock distribution and recovery.

1. Introduction

Ultrafast laser sources are of strong interest in various applications such as optical clocks [1], length metrology [2], optical communications [3] and high performance data centers [4]. Driven by the huge demand to utilize the vast amount of bandwidth offered by optical fibers, wavelength-division multiplexing (WDM) solutions have evolved quickly, since they are much more energy-efficient relative to using multiple single-wavelength laser sources [5]. Silicon photonics, benefiting from the mature complementary metal-oxide-semiconductor (CMOS) industry, meets the requirements to develop photonic integrated circuits (PICs) [6]. In contrast to growing passive photonic component integration on silicon, the development of on-chip WDM light sources is limited by the inherent indirect-bandgap nature of silicon; nevertheless, during the past decade, huge breakthroughs in growing quantum dot (QD) lasers on Si have demonstrated the potential of these nano-objects to be an ideal active medium owing to the charge carrier confinement in three spatial dimensions. Low relative intensity noise [7], narrow spectral linewidth [8, 9], high tolerance to external feedback [10], and remarkable temperature stability [11] have been demonstrated, amongst other attributes. In this context, monolithic mode-locked lasers (MLL) with QD gain regions are reliable sources for generating ultra-short pulses, which are useful for a large number of applications such as communications, metrology, and clock distribution in future computer processors. In signal processing, optical pulses with short picosecond pulse duration and multi-gigahertz repetition rates are needed. Furthermore, a low timing jitter is also required to prevent errors arising from the ambiguity between successive neighboring pulses. Indeed, any error in timing appears as an error in the sampled signal itself, greatly reducing the dynamic range of the sampled signal. To this end, mode-locking technique is ideal solution to generate ultra-short pulses to overcome this issue [12–14]. In particular, passively mode-locked

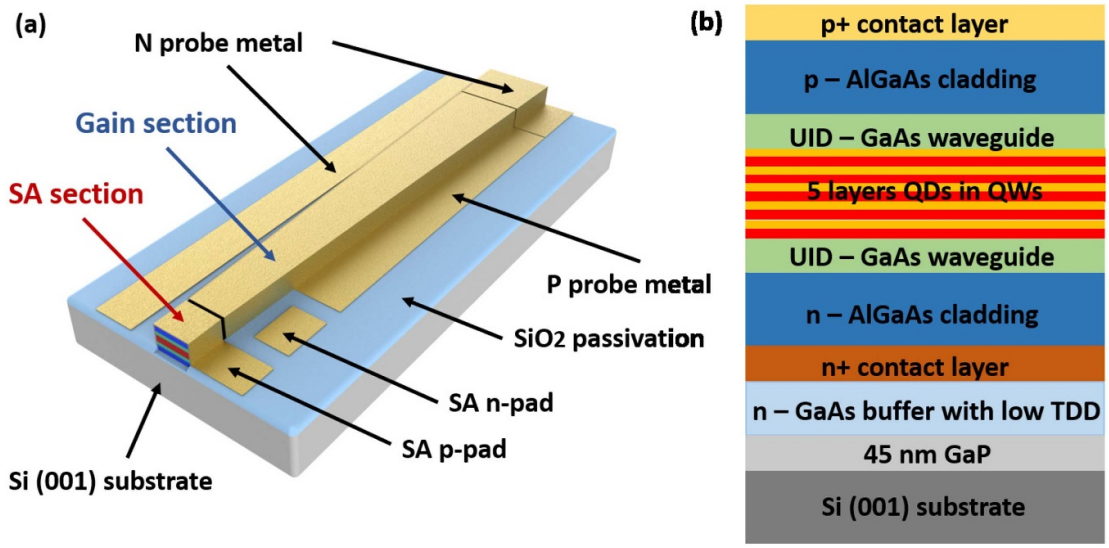

Figure 1. Schematic diagram of (a) the 20 GHz silicon QD-MLL (not to scale) and (b) the corresponding epitaxial structure of device.

QD-MLLs operating with a saturable absorber (SA) are efficient pulsed light sources [15] without the need of synchronization by external driver circuits. As opposed to active mode-locking, these devices are much more robust, simple, and compact [16]. In addition, when QDs are used as the gain media, they produce a low threshold and a low noise performance. In this case, these devices can be implemented as an efficient source for optical clock distribution and ultra-short pulse generation. Recent achievements demonstrate that such lasers with QDs directly grown on silicon are useful for direct modulation of light [17, 18], for self mode-locking [19], high transmission capacity [20], and ultra-narrow RF linewidth [21]. Such findings are thus desired for WDM applications [22, 23].

This paper reports on an initial investigation of optical feedback in a 20 GHz passive QD-MLL epitaxially grown on silicon. The linewidth enhancement factor (also known as the α_H factor) is first investigated because it is a key parameter in semiconductor laser physics, which influences laser performance such as feedback sensitivity [24] and spectral linewidth [9]. In this work, our measurements reveal that the effective α_H factor increases dramatically with the electric field, i.e. the reverse voltage applied to the SA. This increase influences the mode-locking performance as recently observed in a QD comb laser [25]. Then, we focus on the QD-MLL stabilization based on an external optical feedback control loop. In the context of integrated photonics, the external reflection sensitivity of an on-chip light source should be carefully taken into account, as even a small backreflection could be detrimental to laser operation stability hence driving it into severe dynamical instabilities such as coherence collapse [26]. From a theoretical viewpoint, the impact of the reflection sensitivity on QD-MLLs has been studied extensively [21, 27]. In addition, prior experimental studies on QD-MLLs demonstrated that external optical feedback is able to influence the laser dynamics and enhance device performance through reducing the phase noise and decreasing timing jitter [28, 29]. In particular, it is known that when a MLL is driven in the integer resonant optical feedback condition, the RF linewidth is shrunk hence allowing a reduction of the timing jitter [30]. In this paper, the initial experiments demonstrate that both the repetition rate and the RF linewidth are influenced by different feedback conditions which can be identified owing to the inclusion of a sub-picosecond delay line. A substantial reduction of the RF linewidth is obtained under the stable resonant operation for which the external cavity length is a multiple of the optical cavity length of the QD-MLL. These results bring further insights in the understanding of silicon QD-MLLs, which contribute to the development of future large-scale silicon PIC applications requiring low power consumption and high-speed transmission.

2. Description of the device

The QD-MLL studied in this paper was directly grown on a CMOS compatible silicon substrate by solid-source molecular beam epitaxy. Figure 1(a) depicts the schematic diagram of the device. The total length of the QD-MLL was designed to be 2048 μm, which corresponds to a 20 GHz fundamental repetition frequency. The ridge width of the device was designed to be monotonically tapered from 3 μm to 6 μm with a SA section of 5% of the cavity in this study. The isolation length between the gain and the SA was 10 μm

with an isolation resistance around 15 kΩ. A detailed schematic illustrating the epitaxial structure is shown in figure 1(b). The active region of the device consists of a five-layer chirped InAs/InGaAs dots-in-a-well structure spaced by 37.5 nm thick p-type modulation doped GaAs barrier layers. The chirped design aims at broadening the full width half maximum of the gain spectrum while maintaining a flat QD optical gain profile. The active region is sandwiched by an upper and lower unintentionally doped (UID) 50 nm GaAs waveguide and clad by a 1400 nm n-type lower and p-type upper AlGaAs layer and 300 nm p-type top contact layer and 1000 nm n-type bottom contact layer. The GaAs buffer was grown on a GaP/Si template ultimately achieving a low threading dislocation density (TDD) value of $7\times 10^{6}\mathrm{cm}^{-2}$. A 10 nm $5\times 10^{17}\mathrm{cm}^{-3}$ p-modulation doped GaAs layer was introduced to the spacers to help improve the gain and temperature performance of the device [11, 31]. More detailed device epitaxial layer and fabrication process information can be found elsewhere [20].

3. Static characterizations

3.1. Mode-locking effect and conditions

Figure 2(a) depicts the evolution of the optical output power with respect to both the SA bias voltage and the bias current applied to the gain section. All measurements in this paper were taken at 20° C. The evolution of the threshold current I_{th} marked by the yellow dashed line is found to slightly increase from 80 to 85 mA when the reverse voltage is varied from 0 V to -5 V; the output power also decreases at higher reverse voltages. Such effects have been observed on another device with the same structure [20] and are due to the higher internal loss caused from the larger absorption in the SA. The marked purple and red bullets correspond to the laser operating conditions applied in the feedback experiments, which will be discussed in section 4.2. The spectral net modal gain G_{net} below threshold measured by amplified spontaneous emission (ASE) method [32] is shown in figure 2(b). Ensuring the device was operated on the optimum mode-locking condition with -5 V biased on the SA, the values of G_{net} consistently enlarge with the bias current from $0.94\times I_{th}$ to I_{th} and the gain peak is near 1257 nm. Therefore, by following Lau and Paslaski's model [30, 33] and subtracting the absorption of the SA above threshold, we can trace the G_{net} variations with bias current increased from below to above threshold. Figure 2(c) depicts the evolution of G_{net} of the mode at 1257 nm as a function of bias current with -5 V applied to the SA. Like any semiconductor laser, the G_{net} increases linearly with current below threshold and clamps once the threshold is reached.

It is worth stressing that the mode-locking conditions of the studied device having a short absorber section (5% of total cavity length) and a tapered gain section needs to be satisfied. Indeed, it was found that a QD-based device with a short SA section has the possibility of not realizing mode-locking [34]. A strict qualitative criteria indicates the necessary conditions for mode-locking without self-pulsation can be expressed as follows [35]:

$$\frac{aL_a}{gL_g} > 10\left(\frac{\frac{dg}{dI}}{\frac{dg}{dI}\Big|_{g=0}}\right)^2 \tag{1}$$

where a is the unsaturated absorption of the SA, g is the modal gain of the gain section, and L_g and L_a are the lengths of the gain section and the absorber section, respectively. I is the bias current; hence, the differential gain is described as dg/dI and therefore the transparency is described as $(dg/dI)|_{g=0}$. The latter is used to give an estimate of the differential absorption within the SA, which is difficult to be measured directly [36]. Without measuring the threshold modal gain, it can be calculated by $g = (aL_a+(\alpha_i+\alpha_m)L)/L_g$, with L, α_i, and α_m being the total cavity length, the internal loss, and the mirror loss, respectively. In addition, at threshold, G_{net} should be zero and α_m is equal to 5.6 cm^{-1}. The variation of g is equivalent to the variation of G_{net} [37]. Assuming linear variation of G_{net} below threshold ensures a constant differential gain, we can therefore transform equation (1) into:

$$\frac{aL_a}{gL_g} > 10\left(\frac{\frac{dG_{net}}{dI}\Big|_{I>I_{th}}}{\frac{dG_{net}}{dI}\Big|_{I<I_{th}}}\right)^2. \tag{2}$$

Figure 2(d) depicts the spectral absorption of the SA measured on another device with similar structure. In this work, the modal total loss is calculated by subtracting the mirror loss from the threshold modal gain measured by Cassidy method [38]. The α_i is measured at 6 cm^{-1} without reverse voltage applied to the SA (red, marked by black dashed line), hence the absorption induced by the SA can be calculated by deducting α_i from the total loss value for all the reverse voltages at the relevant wavelength. Our results reveal that a close to peak modal gain is found to slightly increase with the reverse voltage from 3 cm^{-1} (without voltage

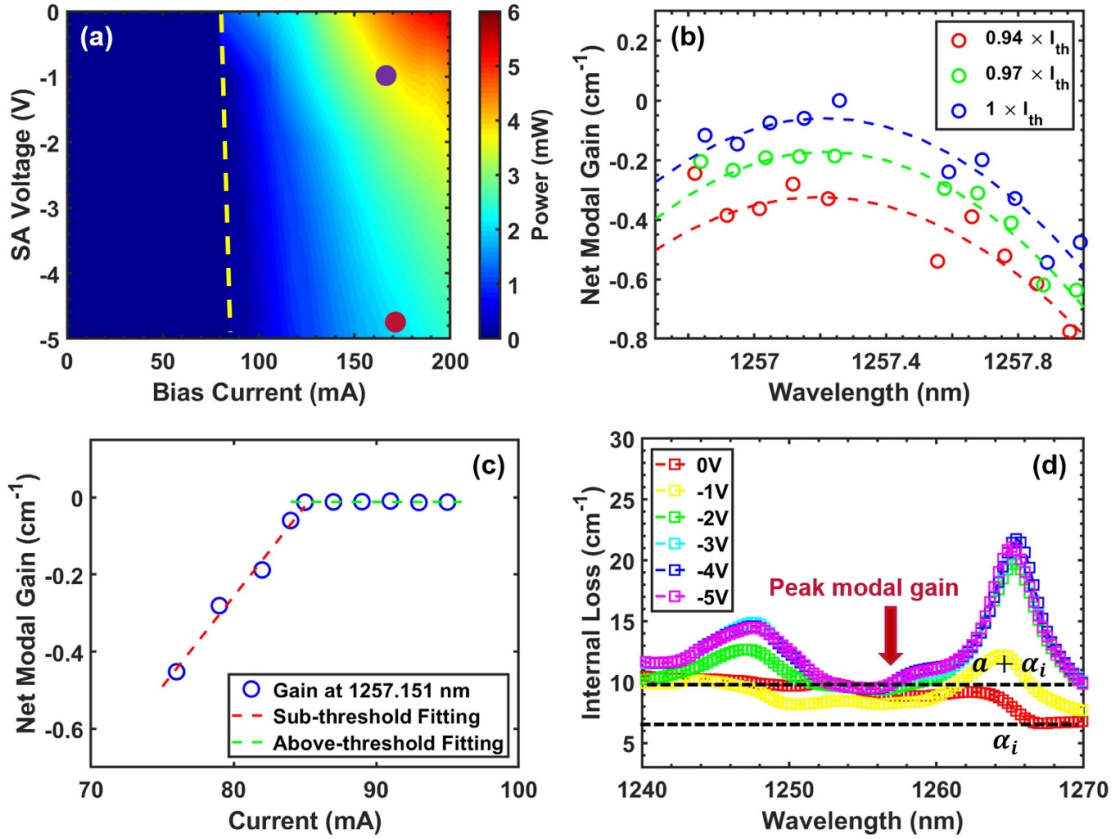

Figure 2. (a) Mapping of the lasing power under different reverse voltages on the SA and bias current conditions. The yellow dashed line (– – – –) represents the evolution of the laser threshold with the reverse voltage. The purple and red bullets (●) correspond to the device operation conditions applied in the feedback experiments introduced in this paper hereafter. (b) The spectral net modal gain G_{net} below threshold and (c) G_{net} at the gain peak as a function of bias current I when SA voltage was biased at -5 V. The fittings of differential gain dG_{net}/dI below and above threshold are marked by red and green dashed lines, respectively. (d) The measured total internal loss on another device with similar structure, with reverse voltage on the SA from 0 V to -5 V.

Table 1. Parameter values for the mode-locked laser simulation.

Parameter	Value $V_{SA}=0$ V	$V_{SA}=-1$ V	$V_{SA}=-5$ V	Units
λ_m	1257	1257	1257	nm
α_m	5.6	5.6	5.6	cm^{-1}
α_i	6	6	6	cm^{-1}
a	3	4	6	cm^{-1}
g	12.4	12.4	12.5	cm^{-1}
L_g	1 945.6	1 945.6	1 945.6	μm
L_a	102.4	102.4	102.4	μm
dG_{net}/dI at $I > I_{th}$	3.78×10^{-2}	3.31×10^{-2}	7.56×10^{-2}	$cm^{-1}mA^{-1}$
dG_{net}/dI at $I < I_{th}$	5.7	4.3	3.9	$cm^{-1}mA^{-1}$
aL_a/gL_g	1.21×10^{-2}	1.61×10^{-2}	2.39×10^{-2}	
$10 \times [(dg/dI)/(dg/dI\|g=0)]^2$	4.42×10^{-4}	5.91×10^{-4}	3.75×10^{-3}	

on the SA) to 6 cm^{-1} (reverse voltage on the SA beyond −2 V). All the parameters relating to equation (2) with the case of 0 V, −1 V and −5 V applied on the SA are listed in table 1. All the cases satisfy equation (2) which means that the device is mode-locked for the operating conditions in this study.

3.2. Linewidth enhancement factor

It is known that the reverse bias voltage on the SA is able to influence the mode-locking [20, 39]. Based on that, the influence of the absorption effect on other laser physics is worth considering. To this end, we go a step beyond by investigating the influence of SA voltage on the α_H factor of the MLL. The α_H factor is a gain medium parameter to describe the carrier density induced change of modal gain and refractive index in the

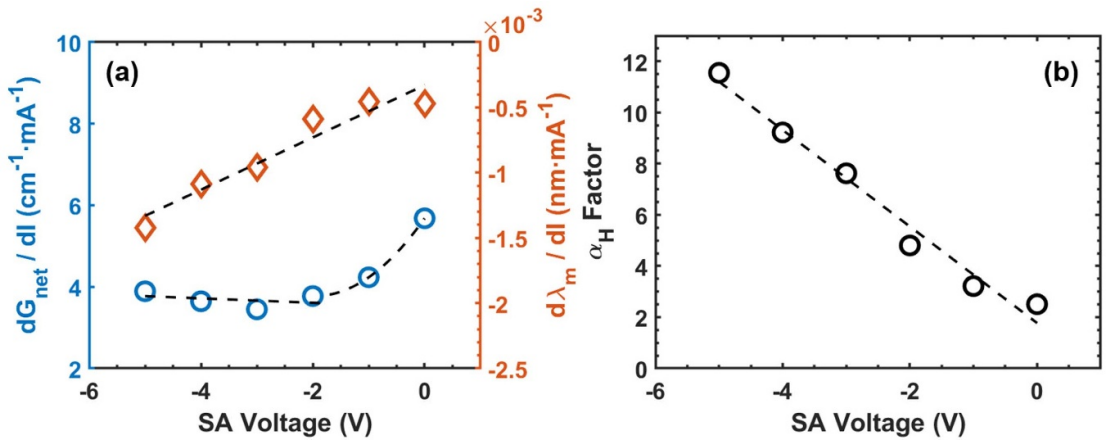

Figure 3. The measured (a) modal differential wavelength $d\lambda_m/dI$ (red), the differential gain dG_{net}/dI (blue), and (b) the α_H factor at threshold as a function of the reverse voltage on the SA.

active region. In this work, the effective α_H factor that is extracted from the ASE [32] can be expressed as a function of direct measurable parameters such as [40]:

$$\alpha_H = -\frac{4n\pi}{\lambda_m^2}\frac{d\lambda_m/dI}{dG_{net}/dI}. \tag{3}$$

Here n is the material refractive index, dG_{net}/dI is the differential gain below threshold and $d\lambda_m/dI$ is the differential lasing wavelength at the gain peak. The latter gives an approach to estimate the carrier density dependence of carrier-induced refractive index. With the view of improving the extraction accuracy, a continuous-wave current source is applied to ensure a good optical mode shape, which is then displayed on a 20 pm high resolution optical spectrum analyzer (OSA); however, the modal wavelength red-shift above threshold caused by thermal effects needs to be totally subtracted from the wavelength blue-shift below threshold, in order to calculate the α_H factor from below to threshold.

Figure 3(a) and (b) display the SA reverse voltage dependence of dG_{net}/dI (blue), $d\lambda_m/dI$ (red) and α_H factor at threshold (black). The parameters are extracted for one longitudinal mode near the gain peak. It is found that the α_H factor increases with the reverse voltage; specifically, its value is found to range from 2.5 (without reverse voltage on the SA) to 11.6 (with -5 V applied on the SA). This effect has already been observed in a QD frequency comb laser [25] and can be explained through equation (3). For a low reverse voltage condition below -1 V, both the decrease of dG_{net}/dI and $d\lambda_m/dI$ contribute to enlarging the α_H factor. While at higher voltages beyond -1 V, the values of dG_{net}/dI typically saturate whereas the sustained drop of $d\lambda_m/dI$ is still able to maintain the increase of the α_H factor. Such a finding of the α_H factor dependence on the SA bias provides an understanding of the stability of the device under optical feedback, since a more stable integer resonant operation is observed at lower bias, where the α_H factor of device is typically smaller. Corresponding experimental results are discussed in section 4.2. In addition, it is worth noting that the device in this study is grown from chirped InAs QDs, which give the device a larger α_H factor [41] compared to a normal QD laser grown on silicon [40]. Overall, this result is the first dataset showing the evolution of the linewidth enhancement factor having chirped QDs grown on silicon. Last but not least, it is worth stressing that both the SA section and the gain section have their own α_H factor. In further work, the contribution which each section of such a two-section device has on the effective α_H factor will be investigated.

4. Optical feedback stabilization

4.1. Experimental setup

The experimental setup used for investigating the optical feedback is shown in figure 4. Laser emission is coupled by anti-reflection (AR)-coated lens-end fiber, and 90% of the coupled power is sent to the 7 meter long-delay feedback path, where an optical delay line (ODL) is applied to introduce extra sub-picosecond delay length in the external feedback loop. In the experiments, such a 7 m-long external cavity means that the relaxation oscillation frequency of the laser is well-beyond that of of the external cavity. A backreflector (BKR) combined with a variable optical attenuator is then wired to reflect the light back to laser cavity and change the feedback strength r_{ext}. In this work, r_{ext} is defined as the ratio between the power return to the laser cavity and the free-space emitting power of the laser. To accurately calculate r_{ext} and understand the

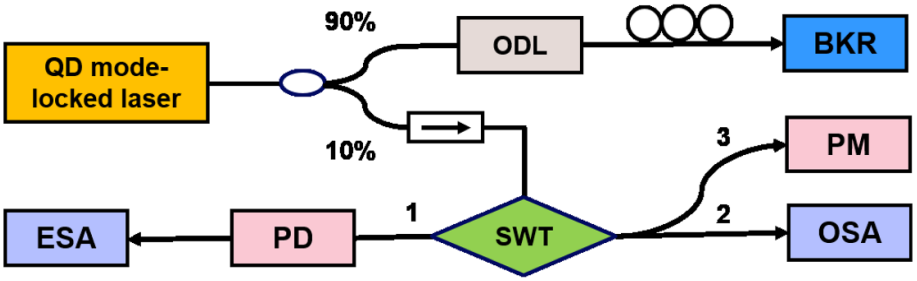

Figure 4. Schematic of the experimental setup used for investigating optical feedback. ODL, optical delay line; BKR, backreflector with variable optical attenuator integrated; SWT, optical switch; OSA, optical spectrum analyzer; PD, photodiode; ESA, electrical spectrum analyzer; PM, powermeter.

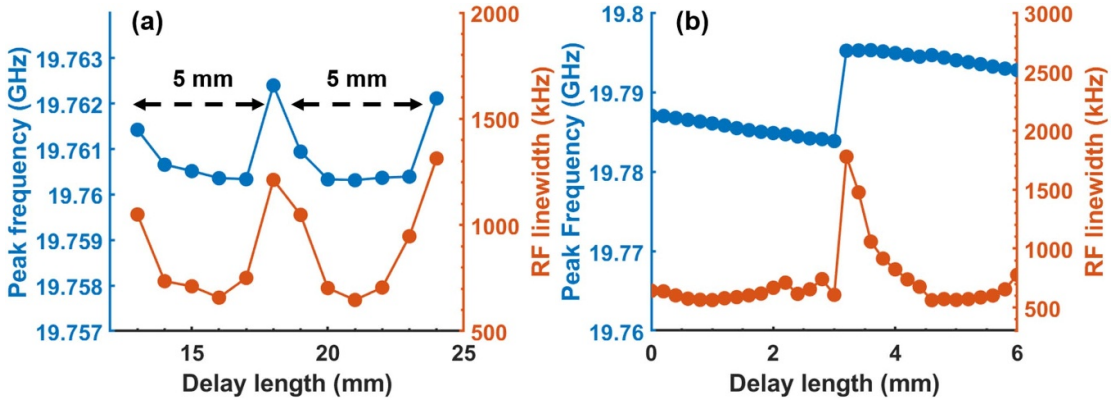

Figure 5. The variation of repetition frequency (blue) and RF linewidth (red) as a function of change in external cavity length, under -35 dB feedback strength r_{ext}. Device operated at twice threshold, with reverse voltage applied to the SA at (a) -1 V and (b) -5 V, respectively.

effects of the optical feedback, the losses from the fiber coupling and in the fiber setup are taken into account; furthermore, a polarization controller is inserted in the external cavity to compensate for the polarization rotation in the fiber. The remaining 10% of coupled light is transferred to an optical switch (SWT) where the signal can be swapped between the powermeter (PM) and the optical and electrical spectrum analyzer (OSA and ESA) for further analysis. The behavior of mode-locked lasers strongly depends on the ratio of the external cavity length (L_{ext}) to the device cavity length (L_{cav}). To this end, the ODL is absolutely vital in order to access both the stable resonant condition namely the integer case and the nonresonant conditions. The former is from a technological viewpoint the most important regime where the RF linewidth can be substantially reduced; whereas, the latter leads to a much broader linewidth that can be a possible precursor towards more severe dynamical instabilities. Practically, the optimum regime is reached for $L_{ext}/L_{cav} \in N$ (N is integer).

4.2. Results and discussions

To understand the influence of external cavity length on the laser performance, figure 5 depicts the QD-MLL peak frequency and RF linewidth as a function of optical delay line length under -35 dB feedback strength, r_{ext}, with the device operated at twice threshold with -1 V (a) and -5 V (b) applied to the SA. Note that such operating conditions marked by purple and red bullets shown in figure 2(a) match the mode-locking criteria discussed in section 3.1. In both cases, finely varying the sub-picosecond delay length allows one to track the evolution of both the repetition frequency and the RF linewidth.

Our results demonstrate that a large reduction of RF linewidth takes place in the optimum feedback condition, which corresponds to the integer resonant operation when the optical length of the external cavity is a multiple of that of the laser cavity [27, 42]. In both cases shown in figure 5, a variation of delay length induces synchronous periodic undulations on the repetition frequency (blue) and the RF linewidth (red), where the periodicity is approximately 5-mm. This length introduces a time delay of ~ 50 ps in free space, which corresponds to the MLL repetition frequency. The periodic enlargements of the RF linewidth take place in the nonresonant operation, which is reached when the optical lengths of the cavities are arbitrary (i.e. $L_{ext}/L_{cav} \notin N$). In the case of -1 V biased on the SA, the minima of RF linewidth are found at L_{ext}/L_{cav}

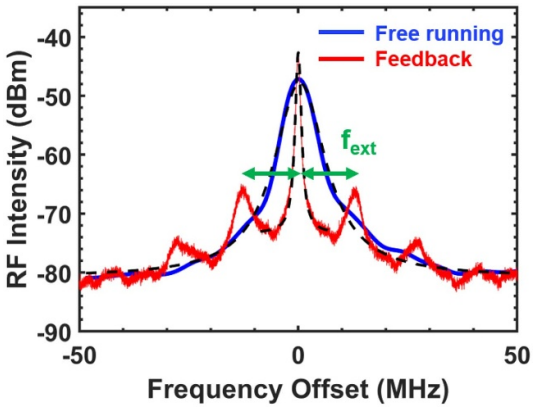

Figure 6. RF line at ~ 20 GHz at free running operation (blue) and that at integer resonant optical feedback operation (red),with -5 V biased on the SA.

equal to 1386 and 1387, whereas the maximum is found at L_{ext}/L_{cav} equal to 1 386.4. Same finding is still valid for the case of -5 V applied to the SA. Despite that, it is important to stress that a low α_H factor should produce a more stable integer resonant operation and increase the critical external reflection related to the occurrence of dynamical instabilities (e.g. coherence collapse). Thus, the smaller α_H factor encountered at low reverse voltage remains better to stabilize both the RF linewidth and the repetition frequency in integer resonant operation. As shown in figure 5, in the case of -1 V on the SA, the device also exhibits a smaller feedback induced variation in the repetition frequency (~ 3 MHz) than that in the case of -5 V applied to the SA (~ 11 MHz). This effect is known to be mainly attributed to the refractive index change through the plasma effect in the active region [43, 44].

Ensuring the device is operated in the integer resonant condition, the RF linewidth is indeed strongly reduced by a factor of 8 down to about 520 kHz against 4.2 MHz under free-running operation, which is shown in figure 6, by setting -5 V on the SA. The ~ 14 MHz spacing side-modes from the fundamental mode-locked frequency results from the 7 m-long external cavity. From the RF linewidth, the pulse-to-pulse rms timing jitter can be expressed as follows:

$$\sigma_{pp} = T\sqrt{\frac{\Delta\nu NT}{2\pi}} \tag{4}$$

where $\Delta\nu$ is the 3-dB RF linewidth and N is the number of periods between the two compared pulses. The reduction of RF linewidth decreases the pulse-to-pulse rms timing jitter. Applying equation (4), the 8-fold RF linewidth reduction under integer resonant feedback operation decreases σ_{pp} by a factor of 2.8 to 108 fs/cycle. In addition, the RF linewidth reduction under optical feedback is observed for all bias voltages in this study (from 0 V to -5 V). Last but not least, it is worth noticing that this reduction of the RF linewidth under optical feedback is illustrated by conducting experiments on a QD-MLL having a short SA section i.e. $L_a/L = 5\%$. Indeed, it is known that the optimum free-running mode-locking performance are obtained for QD devices with L_a/L ratios between 10% and 15%. Such a lower efficiency of mode-locking can possibly explain the degradation of the performance and the large RF linewidth at free running operation of the device in this study [34], when it is compared with the ultra-low RF linewidth demonstrated on a device of similar structure [20].

5. Conclusions

In this work, we have investigated the α_H factor and performance of a QD-MLL on silicon under optical feedback. These results show that the effective α_H factor is strongly affected by the bias on the SA and its value increases with the reverse voltage applied to the SA. In the stable-resonant feedback condition, the RF linewidth is strongly reduced. To summarize, this work brings novel insights in the understanding of silicon QD-MLLs physics that are useful for designing high performance optical clocks, frequency comb generators, or ultra-low noise photonic oscillators for high-speed dense WDM PICs in optical interconnects and datacom applications.

Acknowledgments

Authors acknowledge the financial support of Advanced Research Projects Agency-Energy contract HR0011-19-C-0083 and the Institut Mines-Télécom.

ORCID iDs

Bozhang Dong https://orcid.org/0000-0001-5826-6723
Jianan Duan https://orcid.org/0000-0001-7710-4287

References

[1] Rosenband T *et al* 2008 Frequency ratio of Al+ and Hg+ single-ion optical clocks; metrology at the 17th decimal place *Science* **319** 1808–12
[2] Coddington I, Swann W C, Nenadovic L and Newbury N R 2009 Rapid and precise absolute distance measurements at long range *Nature Photon.* **3** 351–6
[3] Wada O 2004 Femtosecond all-optical devices for ultrafast communication and signal processing *New J. Phys.* **6** 183–183
[4] Vujicic V, Calö C, Watts R, Lelarge F, Browning C, Merghem K, Martinez A, Ramdane A and Barry L P 2015 Quantum dash mode-locked lasers for data centre applications *IEEE J. Selec. Top. Quantum Electron.* **21** 53–60
[5] Stern B, Zhu X, Chen C P, Tzuang L D, Cardenas J, Bergman K and Lipson M 2015 On-chip mode-division multiplexing switch *Optica* **2** 530–5
[6] Jones R, Doussiere P, Driscoll J B, Lin W, Yu H, Akulova Y, Komljenovic T and Bowers J E 2019 Heterogeneously integrated InP/silicon photonics: fabricating fully functional transceivers *IEEE Nanotechnol. Magazine* **13** 17–26
[7] Vujicic V *et al* 2017 Mitigation of relative intensity noise of quantum dash mode-locked lasers for PAM4 based optical interconnects using encoding techniques *Opt. Express* **25** 20–9
[8] Lu Z G *et al* 2018 High performance InAs/InP quantum dot 34.462-GHz C-band coherent comb laser module *Opt. Express* **26** 2160–7
[9] Duan J, Huang H, Lu Z G, Poole P J, Wang C and Grillot F 2018 Narrow spectral linewidth in InAs/InP quantum dot distributed feedback lasers *Appl. Phys. Lett.* **112** 121102
[10] Duan J, Huang H, Dong B, Jung D, Norman J C, Bowers J E and Grillot F 2019 1.3- μ m reflection insensitive InAs/GaAs quantum dot lasers directly grown on silicon *IEEE Photonics Technol. Lett.* **31** 345–8
[11] Huang H, Duan J, Dong B, Norman J, Jung D, Bowers J E and Grillot F 2020 Epitaxial quantum dot lasers on silicon with high thermal stability and strong resistance to optical feedback *APL Photonics* **5** 016103
[12] Zhang H, Tang D, Knize R J, Zhao L, Bao Q and Loh K P 2010 Graphene mode locked, wavelength-tunable, dissipative soliton fiber laser *Appl. Phys. Lett.* **96** 111112
[13] Lin Y-H, Yang C-Y, Liou J-H, Chin-Ping Y and Lin G-R 2013 Using graphene nano-particle embedded in photonic crystal fiber for evanescent wave mode-locking of fiber laser *Opt. Express* **21** 16763–76
[14] Lin Y-H *et al* 2015 Using n-and p-type Bi_2Te_3 topological insulator nanoparticles to enable controlled femtosecond mode-locking of fiber lasers *Acs Photonics* **2** 481–90
[15] Weiner A M 2009 *Ultrafast Optics* (New York: Wiley)
[16] Haus H A 2000 Mode-locking of lasers *IEEE J. Selec. Top. Quantum Electron.* **6** 1173–85
[17] Jhang Y-H, Mochida R, Tanabe K, Takemasa K, Sugawara M, Iwamoto S and Arakawa Y 2016 Direct modulation of 1.3 μm quantum dot lasers on silicon at 60° C *Opt. Express* **24** 18428–35
[18] Inoue D, Jung D, Norman J, Wan Y, Nishiyama N, Arai S, Gossard A C and Bowers J E 2018 Directly modulated 1.3 μm quantum dot lasers epitaxially grown on silicon *Opt. Express* **26** 7022–33
[19] Liu S, Jung D, Norman J C, Kennedy M J, Gossard A C and Bowers J E 2018 490 fs pulse generation from passively mode-locked single section quantum dot laser directly grown on on-axis GaP/Si *Electron. Lett.* **54** 432–3
[20] Liu S, Wu X, Jung D, Norman J C, Kennedy M J, Tsang H K, Gossard A C and Bowers J E 2019 High-channel-count 20 GHz passively mode-locked quantum dot laser directly grown on si with 4.1 Tbit/s transmission capacity *Optica* **6** 128–34
[21] Auth D, Liu S, Norman J, Bowers J E and Breuer S 2019 Passively mode-locked semiconductor quantum dot on silicon laser with 400 Hz RF line width *Opt. Express* **27** 27256–66
[22] Müller J *et al* 2015 Silicon photonics WDM transmitter with single section semiconductor mode-locked laser *Adv. Opt. Technol.* **4** 119–45
[23] Kurczveil G, Seyedi M A, Liang D, Fiorentino M and Beausoleil R G 2018 Error-free operation in a hybrid-silicon quantum dot comb laser *IEEE Photonics Technol. Lett.* **30** 71–4
[24] Dong B, Duan J, Shang C, Huang H, Sawadogo A B, Jung D, Wan Y, Bowers J E and Grillot F 2019 Influence of the polarization anisotropy on the linewidth enhancement factor and reflection sensitivity of 1.55-μm InP-based InAs quantum dash lasers *Appl. Phys. Lett.* **115** 091101
[25] Dong B, Huang H, Duan J, Kurczveil G, Liang D, Beausoleil R G and Grillot F 2019 Frequency comb dynamics of a 1.3 μm hybrid-silicon quantum dot semiconductor laser with optical injection *Opt. Lett.* **44** 5755–8
[26] Erneux T and Glorieux P 2010 *Laser Dynamics* (Cambridge: Cambridge University Press)
[27] Avrutin E A and Russell B M 2009 Dynamics and spectra of monolithic mode-locked laser diodes under external optical feedback *IEEE J. Quantum Electron.* **45** 1456–64
[28] Lin C-Y, Grillot F, Li Y, Raghunathan R and Lester L F 2011 Microwave characterization and stabilization of timing jitter in a quantum-dot passively mode-locked laser via external optical feedback *IEEE J. Selec. Top. Quantum Electron.* **17** 1311–17
[29] Nikiforov O, Jaurigue L, Drzewietzki L, Lüdge K and Breuer S 2016 Experimental demonstration of change of dynamical properties of a passively mode-locked semiconductor laser subject to dual optical feedback by dual full delay-range tuning *Opt. Express* **24** 14301–10
[30] Lin C-Y, Grillot F, Naderi N A, Li Y and Lester L F 2010 rf linewidth reduction in a quantum dot passively mode-locked laser subject to external optical feedback *Appl. Phys. Lett.* **96** 051118

[31] Liu S, Norman J, Dumont M, Jung D, Torres A and Gossard A C 2019 and J E Bowers. High-performance o-band quantum-dot semiconductor optical amplifiers directly grown on a cmos compatible silicon substrate *ACS Photon.* **6** 2523–9
[32] Osinski M and Buus J 1987 Linewidth broadening factor in semiconductor lasers–An overview *IEEE J. Quantum Electron.* **23** 9–29
[33] Palaski J and Lau K Y 1991 Parameter ranges for ultrahigh frequency mode locking of semiconductor lasers *Appl. Phys. Lett.* **59** 7–9
[34] Liu S, Norman J C, Jung D, Kennedy M J, Gossard A C and Bowers J E 2018 Monolithic 9 GHz passively mode locked quantum dot lasers directly grown on on-axis (001) si *Appl. Phys. Lett.* **113** 041108
[35] Lin C-Y, Xin Y-C, Naderi N A, Chiragh F L and Lester L F 2009 Monolithic 1.58-micron InAs/InP quantum dash passively mode-locked lasers *Physics and Simulation of Optoelectronic Devices Xvii* (Bellingham, WA: SPIE) p 721118
[36] Lin C-Y, Xin Y-C, Li Y, Chiragh F and Lester L F 2009 Cavity design and characteristics of monolithic long-wavelength InAs/InP quantum dash passively mode-locked lasers *Opt. Express* **17** 19739–48
[37] Hakki B W and Paoli T L 1975 Gain spectra in GaAs double- heterostructure injection lasers *J. Appl. Phys.* **46** 1299–306
[38] Cassidy D T 1984 Technique for measurement of the gain spectra of semiconductor diode lasers *J. Appl. Phys.* **56** 3096–9
[39] Rafailov E U, Cataluna M A and Sibbett W 2007 Mode-locked quantum-dot lasers *Nature Photon.* **1** 359–401
[40] Duan J, Huang H, Jung D, Zhang Z, Norman J, Bowers J E and Grillot F 2018 Semiconductor quantum dot lasers epitaxially grown on silicon with low linewidth enhancement factor *Appl. Phys. Lett.* **112** 251111
[41] Kim K C, Han I K, Lee J I and Kim T G 2010 Gain-dependent linewidth enhancement factor in the quantum dot structures *Nanotechnology* **21** 134010
[42] Solgaard O and Lau K Y 1993 Optical feedback stabilization of the intensity oscillations in ultrahigh-frequency passively modelocked monolithic quantum-well lasers *IEEE Photonics Technol. Lett.* **5** 1264–7
[43] Bennett B R, Soref R A and Del Alamo. J A 1990 Carrier-induced change in refractive index of InP, GaAs and InGaAsP *IEEE J. Quantum Electron.* **26** 113–22
[44] Passerini M, Sorel M and Laybourn P J R 2004 Optimisation and regime characterisation of monolithic semiconductor mode-locked lasers and colliding-pulse mode-locked lasers at microwave and millimetre-wave frequencies *IEE Proc. Optoelectron.* **151** 508–12